

CORRESPONDENCE

Open Access



# Spatial imaging unlocks the potential of charting multiple myeloma and extramedullary disease

Vanessa Desantis<sup>1</sup>, Alessandro Andriano<sup>1</sup>, Tim Düking<sup>2</sup>, Olga Hartwig<sup>2</sup>, Giuseppe Ingravallo<sup>3</sup>, Marta Biondo<sup>4</sup>, Cirino Botta<sup>5</sup>, Roberto Ria<sup>6</sup>, Angelo Vacca<sup>6</sup> and Antonio Giovanni Solimando<sup>6\*</sup>

## Abstract

Extramedullary disease (EMD) in multiple myeloma (MM) represents a significant clinical challenge, with a limited understanding of the spatial architecture and its pathobiological impact. To address this unmet need, we examined 10 matched samples from bone marrow (BM) and cognate EMD sites. This investigation provides critical insights into the distinct features of EMD, offering potential avenues for more effective diagnosis and targeted therapies. To this aim, we employed MACSima™ Imaging Cyclic Staining (MICS) to unveil distinct biomarker expression profiles as companion diagnostics for a personalized therapeutic approach for MM. We observed elevated BCL-2 levels in EMD plasma cells ( $p < 0.0001$ ), indicating the potential of BCL-2 inhibitors to target anti-apoptotic pathways in select cases. The higher expression of EZH2 in EMD compared to BM ( $p < 0.0001$ ) highlights its role in sustaining aggressive tumor phenotypes and supports the use of epigenetic-targeting agents in key situations. In contrast, CD3+T-cell distance was significantly higher in EMD, reflecting impaired immune surveillance ( $p < 0.0001$ ). Across the cohort, our analysis revealed significant differences between BM and EMD regarding the expression and spatial organization of key markers. CD38 expression was markedly reduced in EMD plasma cells ( $p < 0.0001$ ). These findings underscore profound biological heterogeneity in MM and its BM emancipated disease phenotype, emphasizing dysfunctional apoptosis, immune evasion and resistance to CD38-targeting therapies in EMD, conceivably informing future validations. By integrating high-dimensional data, this study provides insights into potential druggable vulnerabilities for crafted interventions, particularly challenging in EMD cases.

**Keywords** Multiple myeloma, MACSima™ imaging system, MICS technology, Extramedullary disease

\*Correspondence:

Antonio Giovanni Solimando  
antonio.solimando@uniba.it

<sup>1</sup>Department of Precision and Regenerative Medicine and Ionian Area (DiMePRe-J), Section of Pharmacology, University of Bari Aldo Moro Medical School, Bari, Italy

<sup>2</sup>Miltenyi Biotec B.V. & Co. KG, Bergisch Gladbach, Germany

<sup>3</sup>Pathological Anatomy Unit, Department of Emergency and Organ Transplantation, University of Bari Aldo Moro, Bari, Italy

<sup>4</sup>Department of General Surgery and Medical-Surgical Specialties, University of Catania, Catania, Italy

<sup>5</sup>Department of Health Promotion, Mother and Child Care, Internal Medicine and Medical Specialties, University of Palermo, Palermo, Italy

<sup>6</sup>Internal Medicine Guido Baccelli, University of Bari Aldo Moro Medical School, Bari, Italy



© The Author(s) 2025. **Open Access** This article is licensed under a Creative Commons Attribution-NonCommercial-NoDerivatives 4.0 International License, which permits any non-commercial use, sharing, distribution and reproduction in any medium or format, as long as you give appropriate credit to the original author(s) and the source, provide a link to the Creative Commons licence, and indicate if you modified the licensed material. You do not have permission under this licence to share adapted material derived from this article or parts of it. The images or other third party material in this article are included in the article's Creative Commons licence, unless indicated otherwise in a credit line to the material. If material is not included in the article's Creative Commons licence and your intended use is not permitted by statutory regulation or exceeds the permitted use, you will need to obtain permission directly from the copyright holder. To view a copy of this licence, visit <http://creativecommons.org/licenses/by-nc-nd/4.0/>.

### To the editor,

State of the art microscopy holds significant potential in hematologic malignancies for the visualization and quantification of molecules within their native context, providing unprecedented insights into cellular function, tissue architecture, cellular composition and cell-to-cell interaction [1].

### Introduction

Despite advances in multiple myeloma (MM) prognosis, extramedullary disease (EMD) remains a challenge, with stagnant survival rates [2]. Traditional diagnostic and monitoring approaches of MM rely heavily on histopathology and bulk analyses, often failing to capture the spatial heterogeneity and the microenvironmental interactions. Recent advancements in companion diagnostics, including highly multiplexed imaging techniques and spatially resolved transcriptomics, have begun to address these limitations [3]. By applying MACSima™ imaging cyclic staining (MICS), we aim to generate a comprehensive biological map of protein expression, revealing the architectural distribution of myeloma cells within their physiological ecosystem [4]. To this end, we report original data demonstrating the utility of this approach in dealing with the complexity of bone marrow (BM) niche and identifying key differences between BM and EMD sites.

### Methods

After meticulous preparation of samples, the MICS technology overcomes the unique challenges of the BM [5], ending in a multiplexed staining of 56 markers (see Supplementary Table 1). Analysis of high-content imaging data is refined by computational tools provided by proprietary software followed by statistical validation (see Supplementary Materials and Methods 1). Biological material included BM biopsies and paired EMD tissue specimens for a total of 10 samples from 5 newly diagnosed MM patients (see Supplementary Table 2), analyzing an overall number of 231,186 cells of which 105,047 were annotated as Plasma cells (PCs).

### Results and discussion

The utility of MICS technology stems from the identification and characterization of BM niche and EMD site as visually presented in Fig. 1A-T and Supplementary Figs. 1–2. After batch correction, data integration, and cell type annotation, we identified 14 distinct cell types in the BM and 9 in the EMD sites (Fig. 1D, H, N, S and Supplementary Fig. 3).

This approach is instrumental to a deeper identification of expression patterns of PCs, while considering the bystander microenvironment heterogeneity at a single cell level. Expression levels of drug resistance markers

in an illustrative patient's paired samples uncovered enhanced expression of BCL-2 and EZH2 at the extramedullary sites ( $p < 0.001$ ) as shown in Fig. 2A-B and C-D. Albeit the need for integrating gene expression analysis in future investigations [6], our findings inform the design of combinational therapies addressing therapeutic opportunities often overlooked by conventional analyses [7, 8].

Moreover, aiming to a deeper profiling of therapeutic vulnerabilities and resistance, we could foresee a decreased CD38 EMD expression (Fig. 2-E,  $p < 0.0001$ ). Immunohistochemistry analysis confirmed CD38 downregulation and BCL-2 and Ki-67 upregulation in EMD compared to BM, supporting the differential expression patterns observed with spatial cyclic immunofluorescence (Fig. 2-F-O, Supplementary Fig. 4,5). Overall, to the best of our knowledge, this is the first direct comparison between matched BM and EMD disease, comparing 56 marker expressions, explaining the worse overall response rate of EMD patients in the era of anti-CD38 monoclonal antibodies [9]. Similarly, the localization of T-cell and macrophages and their interaction with PCs can provide insights into tumor microenvironment (TME) biology and its role in MM pathogenesis [10]. Spatial analysis revealed distinct plasma cell clustering and macrophage infiltration, as shown by cell type assortativity heatmaps (Fig. 2P-R, Supplementary Fig. 6) and a greater distance of PCs from T-cells in the EMD sample ( $p < 0.0001$ ), as shown in Fig. 2S and Supplementary Fig. 6. Similar results can explain the failure of novel therapies like bispecific antibodies and CAR-T cells on EMD patients [11, 12].

### Conclusions

Stemming from high-content data, this methodology offers a deeper understanding of the TME. While the findings provide valuable insights, the absence of transcriptomic data highlight the need for cautious interpretation. Collectively, integrating spatial proteomics using the MICS technology provides distinct biomarker expression profiles as companion diagnostics for a personalized therapeutic approach. Future studies on larger patient cohorts will be essential to further validate the robustness and reproducibility of spatial cyclic immunofluorescence, ensuring its broader applicability as a companion diagnostic tool in MM. The rare but aggressive EMD phenotype could profit the most from similar strategies.

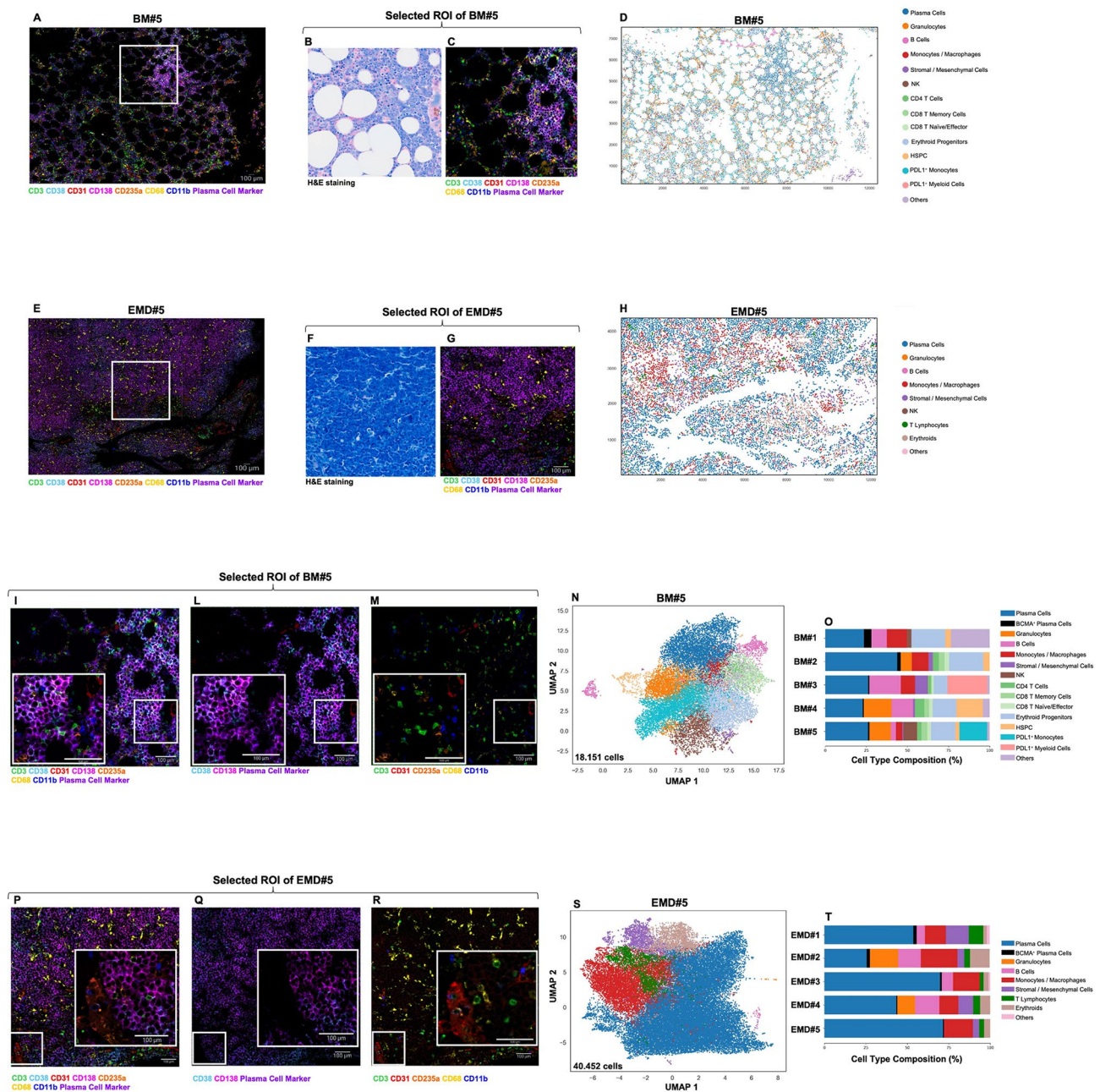


**Fig. 1** Spatial profiling of bone marrow (BM) niche and extramedullary disease (EMD) in multiple myeloma (MM). Fluorescence was optimized for better visualization of cells of interest. Markers selected for this aim were CD138, CD38 and plasma cell marker for plasma cells (PCs), while CD3, CD68, CD11b, CD31 were selected for the tumor microenvironment (TME) component. **A:** Region of interest (ROI) of a BM section showing fluorescence of both PCs and TME. (Scale bar = 100  $\mu$ m). **B-C:** Hematoxylin and eosin (H&E) staining of a selected area of BM from a representative patient (BM#5). Original magnifications  $\times 20$ . **(B)** Matched area showing markers fluorescence of both PCs and the TME component. Original magnifications  $\times 20$ , scale bar = 100  $\mu$ m **(C)**. **D:** Spatial distribution of annotated cell types in BM sample of the representative patient BM#5. **E:** ROI of an EMD section showing PCs and TME component. Scale bar = 100  $\mu$ m. **F-G:** H&E staining of the selected ROI of the EMD representative sample (EMD#5). Original magnifications  $\times 20$  **(F)**. Matched area showing markers fluorescence of both the PCs and the TME component. Original magnifications  $\times 20$ , scale bar = 100  $\mu$ m **(G)**. **H:** Spatial distribution of annotated cell types in EMD sample of the representative patient EMD#5. **I-M:** BM#5 ROI at different magnifications: visualization of all selected markers **(I)**, only selected PCs markers **(L)**, only selected TME markers **(M)** in the selected ROI. Scale bar = 100  $\mu$ m. **N:** UMAP visualization of cell populations in BM#5 (legend on side). **O:** Stacked bar plots showing the cell type composition of all BM samples. Color indicates cell type annotation (legend on side). **P-R:** EMD#5 ROI at different magnifications: visualization of all selected markers **(P)**, only selected PCs markers **(Q)**, only selected TME markers **(R)**. Scale bar = 100  $\mu$ m. **S:** UMAP visualization of cell population in EMD#5. Colors indicate cell type annotation (legend on side). **T:** Stacked bar plots showing the cell type composition of all EMD samples. Color indicates cell type annotation (legend on side)

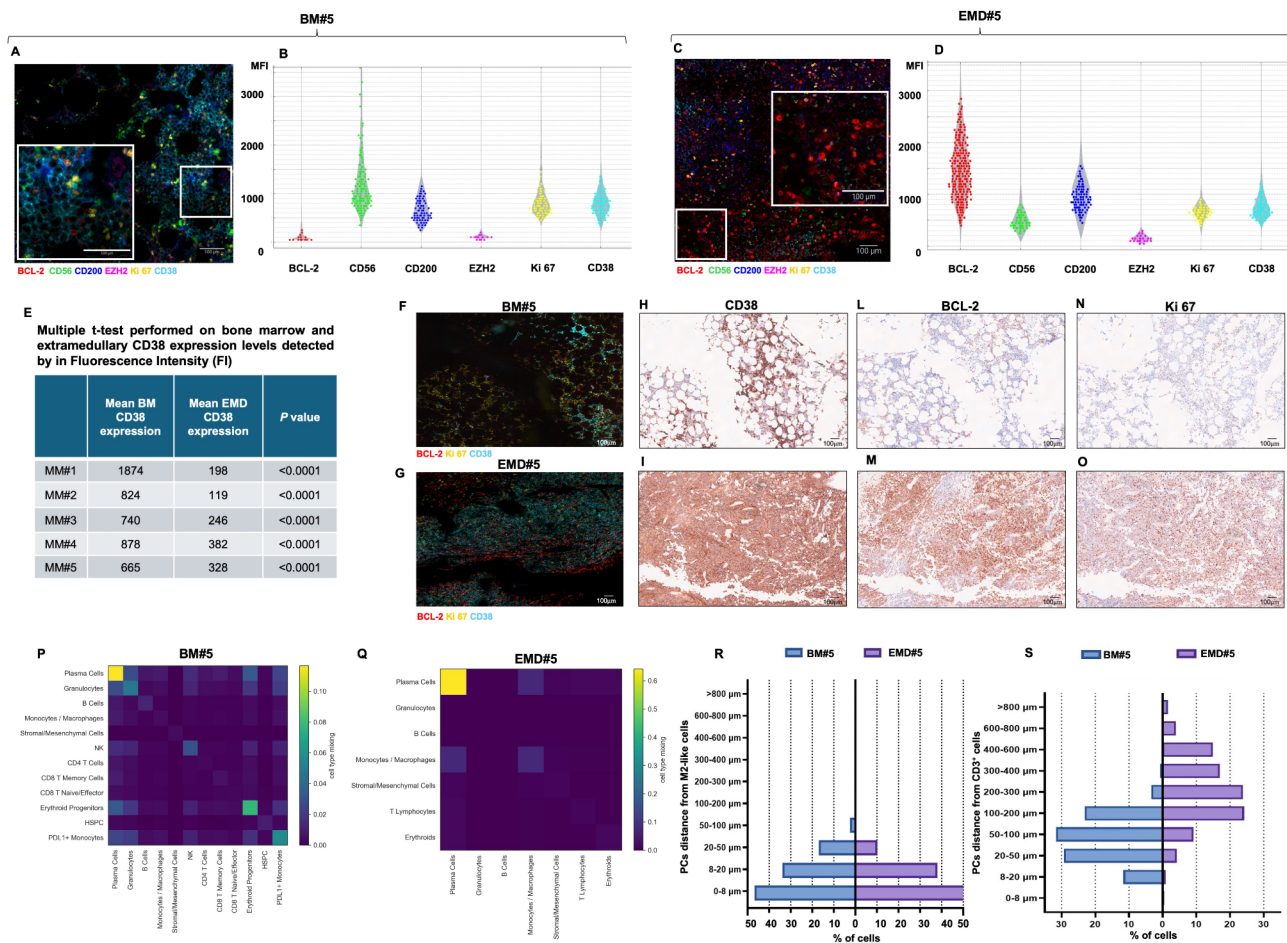


**Fig. 2** Analysis of biomarkers expression and spatial distribution comparing bone marrow (BM) and extramedullary disease (EMD). **A-B**: Visualization of biomarker expressions specific to disease biology (BCL-2, CD56, CD200, EZH2, Ki-67 and CD38) and plasma cells (PCs) expression levels as strip-violin plot after segmentation and annotation in the selected region of interest (ROI) of BM#5 sample. Expression levels of biomarkers between BM PCs and EMD PCs were statistically different ( $p$ -value < 0.0001, Mann-Whitney test). **C-D**: Visualization of biomarker expressions specific to disease biology (BCL-2, CD56, CD200, EZH2, Ki-67 and CD38) and expression levels as strip-violin plot after segmentation and annotation in the selected region of interest (ROI) of EMD#5 sample. Expression levels of biomarkers between BM PCs and EMD PCs were statistically different ( $p$ -value < 0.0001, Mann-Whitney test). **E**: Table summarizing results of statistical analysis regarding data on CD38 expression in a cohort of 5 patients after cell segmentation and PCs annotation: median value of single PCs fluorescence intensity is reported for paired BM and EMD sample. Multiple t-tests were performed and revealed statistically significant differences between samples ( $p$ -value < 0.0001). **F-G**: Visualization by MICS technology of CD38 (light blue), BCL-2 (red) and Ki 67 (yellow) markers in MM#5 paired samples. **H-O**: Immunohistochemistry validation of CD38, BCL-2 and Ki 67 expression both in BM#5 (H-L-N) and EMD#5 (I-M-O). **P-Q**: Cell type assortativity in neighbourhood graphs for MM#5 paired samples. Heatmaps show the fraction of links connecting all possible cell type pairs, indicating cell type mixing. **R-S**: Butterfly graph comparing PCs distance from CD3<sup>+</sup> T-cells (**R**) and M2-like cells (**S**) in representative MM#5 paired samples. The percentage of PCs in the BM (left/blue) and EMD (right/purple) are simultaneously shown at selected distance ranges. Spatial analysis to extract distance values was performed after segmentation and annotation of PCs, T-cells and M2-like cells in each sample. Difference was confirmed as statistically significant ( $p$  < 0.0001, Mann-Whitney test)

#### Abbreviations

BM	Bone marrow
EMD	Extramedullary disease
MM	Multiple myeloma
MICS	MACSima™ imaging cyclic staining
PCs	Plasma cells
TME	Tumor microenvironment

#### Supplementary Information

The online version contains supplementary material available at <https://doi.org/10.1186/s13045-025-01699-x>.

Supplementary Material and Methods 1

Supplementary Table 1

Supplementary Figure 1

Supplementary Figure 2

Supplementary Figure 3

Supplementary Figure 4

Supplementary Figure 5

Supplementary Figure 6

## Supplementary Table 2

**Acknowledgements**

The authors thank Dr. Giorgio Croci for his professional and technical support, valuable discussions and supervision in ensuring the accuracy and quality of the samples used in this study.

**Author contributions**

V.D. and A.G.S. designed the research; V.D., A.A., T.D., O.H., and A.G.S. performed the experiments; A.A., T.D. and A.G.S. were involved in the analysis and interpretation of the data; G.I. performed the pathological analysis; V.D., A.A., M.B., C.B. and A.G.S. wrote the manuscript; G.I., R.R., A.V. supervised the research and revised the manuscript; A.G.S., R.R. and A.V. were involved in patients' enrollment; A.G.S. obtained the informed consent and obtained the primary samples. A.G.S. financially supported the research. All authors approved the manuscript.

**Funding**

This work was supported by the "Fondo per il Programma Nazionale di Ricerca e Progetti di Rilevante Interesse Nazionale—PRIN" (project n.2022ZKKWLW) to A.G.S.; by the Italian network of excellence for advanced diagnosis (INNOVA), Ministero della Salute (code PNC-E3-2022-23683266 PNC-HLS-DA) to V.D. and A.G.S., and by a grant from "Società Italiana di Medicina Interna—SIMI" 2023 Research Award (CAMEL) to A.G.S. This work was also supported by the Italian Association for Cancer Research (AIRC) within the My First AIRC Grant 2020 (n. 24534, 2021/2025) to C.B.

**Data availability**

The data that support the findings of this study are available from the corresponding author upon reasonable request.

**Declarations****Ethics approval and consent to participate**

This study was approved by the Ethics Committee of the University of Bari Medical School (Study No. 7411, Protocol No. 0073322, approved on 26/08/2022 and Study No. 1879, Protocol No. 808 approved on 02/10/2024). All procedures involving human participants were conducted following the ethical standards outlined in the Declaration of Helsinki. Written informed consent was obtained from all enrolled patients before they participated in the study.

**Consent for publication**

All participants provided written informed consent for the publication of anonymized data derived from this study.

**Competing interests**

A.G.S. has received speaker honorariums from Sanofi, Amgen, and AstraZeneca. He has also participated on advisory boards for Pfizer and Menarini. He received travel support for educational purposes from Janssen Cilag. C.B. has served as a speaker or consultant for Amgen, Janssen Cilag, Pfizer, Sanofi Aventis, Takeda, GSK, Oncopeptides. A.V. received speaker honorariums from Pfizer, Sanofi, Bristol Myers Squibb, Takeda, Janssen Cilag, AstraZeneca, Menarini, and Amgen. R.R. has served as a speaker or consultant for Amgen, BMS-Celgene, CSL Behring, Janssen Cilag, Octapharma, Pfizer, Sanofi, Takeda. These potential conflicts of interest do not imply bias or

influence on the authors' opinions or actions. The authors are aware of the importance of transparency in the scientific field and are committed to defending their integrity and the trust in them within the scientific community.

Received: 16 December 2024 / Accepted: 11 April 2025

Published online: 23 April 2025

**References**

1. Roeder T, Baertsch MA, Fitzgerald D, Vöhringer H, Brinkmann BJ, Czernilofsky F, et al. Multimodal and spatially resolved profiling identifies distinct patterns of T cell infiltration in nodal B cell lymphoma entities. *Nat Cell Biol*. 2024;26(3):478–89.
2. Zanwar S, Ho M, Lin Y, Kapoor P, Binder M, Buadi FK, et al. Natural history, predictors of development of extramedullary disease, and treatment outcomes for patients with extramedullary multiple myeloma. *Am J Hematol*. 2023;98(10):1540–9.
3. Rasche L, Chavan SS, Stephens OW, Patel PH, Tytarenko R, Ashby C, et al. Spatial genomic heterogeneity in multiple myeloma revealed by multi-region sequencing. *Nat Commun*. 2017;8(1):268.
4. Robinson MH, Villa NY, Jaye DL, Nooka AK, Duffy A, McCachren SS, et al. Regulation of antigen-specific T cell infiltration and Spatial architecture in multiple myeloma and premalignancy. *J Clin Invest*. 2023;133(15):e167629.
5. Hagos YB, Lecat CSY, Patel D, Mikolajczak A, Castillo SP, Lyon EJ, et al. Deep learning enables Spatial mapping of the mosaic microenvironment of myeloma bone marrow Trephine biopsies. *Cancer Res*. 2024;84(3):493–508.
6. John M, Helal M, Duell J, Mattavelli G, Stanojkowska E, Afrin N, et al. Spatial transcriptomics reveals profound subclonal heterogeneity and T-cell dysfunction in extramedullary myeloma. *Blood*. 2024;144(20):2121–35.
7. Chemlal D, Varlet E, Machura A, Ovejero S, Requirand G, Robert N, et al. EZH2 targeting induces CD38 upregulation and response to anti-CD38 immunotherapies in multiple myeloma. *Leukemia*. 2023;37(9):1925–8.
8. Kumar SK, Harrison SJ, Cavo M, De La Rubia J, Popat R, Gasparetto C, et al. Venetoclax or placebo in combination with bortezomib and dexamethasone in patients with relapsed or refractory multiple myeloma (BELLINI): a randomised, double-blind, multicentre, phase 3 trial. *Lancet Oncol*. 2020;21(12):1630–42.
9. Notarfranchi L, Accardi F, Mancini C, Martella E, Bonomini S, Segreto R et al. CD38 expression by plasma cells in extramedullary multiple myeloma. *Haematologica* [Internet]. 2023 Nov 9 [cited 2024 Dec 9]; Available from: <http://haematologica.org/article/view/haematol.2023.284169>
10. Cencini E, Sicuranza A, Ciofini S, Fabbri A, Bocchia M, Gozzetti A. Tumor-Associated macrophages in multiple myeloma: key role in disease biology and potential therapeutic implications. *Curr Oncol*. 2023;30(7):6111–33.
11. Chari A, Minnema MC, Berdeja JG, Oriol A, Van De Donk NWCJ, Rodríguez-Otero P, et al. Talquetamab, a T-Cell–Redirecting GPRC5D bispecific antibody for multiple myeloma. *N Engl J Med*. 2022;387(24):2232–44.
12. Zanwar S, Sidana S, Shune L, Puglianini OC, Pasvolosky O, Gonzalez R, et al. Impact of extramedullary multiple myeloma on outcomes with Idecabtagene vicleucel. *J Hematol Oncol* *Hematol Oncol*. 2024;17(1):42.

**Publisher's note**

Springer Nature remains neutral with regard to jurisdictional claims in published maps and institutional affiliations.